Frontiers of Physics
https://doi.org/10.1007/s11467-021-1140-3
Front. Phys.
17(4), 43502 (2022)

RESEARCH ARTICLE

Near-field infrared response of graphene on copper substrate

Zhen-Bing Dai[1,3], Gui Cen[1], Zhibin Zhang[2], Xinyu Lv[1], Kaihui Liu[2], Zhiqiang Li[1,†]

[1] *College of Physics, Sichuan University, Chengdu 610065, China*
[2] *School of Physics, Peking University, Beijing 100871, China*
[3] *Department of Physics, Sichuan Normal University, Chengdu 610066, China*
Corresponding author. E-mail: [†] *zhiqiangli@scu.edu.cn*
Received September 1, 2021; accepted December 8, 2021

The electronic properties of graphene are very sensitive to its dielectric environment. The coupling to a metal substrate can give rise to many novel quantum effects in graphene, such as band renormalization and plasmons with unusual properties, which are of high technological interest. Infrared nanoimaging are very suitable for exploring these effects considering their energy and length scales. Here, we report near-field infrared nanoimaging studies of graphene on copper synthesized by chemical vapor deposition. Remarkably, our measurements reveal three different types of near-field optical responses of graphene, which are very distinct from the near-field edge fringes observed in the substrate. These results can be understood from the modification of optical conductivity of graphene due to its coupling with the substrate. Our work provides a framework for identifying the near-field response of graphene in graphene/metal systems and paves the way for studying their novel physics and potential applications.

Keywords near-field infrared response, graphene, copper, graphene/metal

1 Introduction

The strength of Coulomb interaction in graphene is controlled by the effective dielectric constant of the environment [1, 2]. A metal at a short distance can screen the long-range part of the electron-electron interactions in graphene [1, 2], which can lead to changes in Fermi velocity renormalization [3] and electron-phonon coupling strength [3–5]. Moreover, in graphene/h-BN/metal heterostructures screening by metal can significantly modify surface plasmon polaritons in graphene [6–8], yielding acoustic plasmon modes with a linear dispersion, long lifetime and strong field confinement [9–12]. Such heterostructures have been employed to reduce the plasmon velocity of graphene, which enables the probe of nonlocal quantum effects via plasmon imaging [13]. Theoretical studies suggest that graphene directly deposited on metal can host acoustic plasmons with low Landau damping and strongly enhanced vertical confinement compared to samples on dielectric substrates [14, 15]. In terms of applications, graphene/metal structures are of high technological relevance, showing excellent potentials in gas and biological sensing [16–18], photodetectors and optoelectronics [19]. Therefore, the graphene/metal system provides an intriguing platform for exploring novel quantum phenomena in graphene and exploiting them for applications.

Chemical vapour deposition (CVD) on copper surfaces can produce large, continuous and high-quality monolayer graphene films [20–22]. High-resolution angle and lateral resolved photoelectron spectroscopy (nano-ARPES) measurements have shown that single grains of graphene on copper exhibit robust Dirac electronic spectrum with the opening of a mini-gap of 50 meV at the Dirac point [23]. These findings are compatible with theoretical predictions of weak interactions between graphene and the Cu substrate [24, 25], which largely preserves the band structure of graphene. Moreover, the interface between graphene and Cu in these CVD grown samples are atomically flat and cleaner than the interface in transferred samples, in which mechanically exfoliated graphene is transferred and deposited onto a metal film. Therefore, CVD grown graphene on Cu constitutes an excellent system for exploring the physics of graphene coupled to a metal.

2 Experimental

Here, we report a near-field infrared (IR) imaging study of graphene grown on copper substrates employing scattering-type scanning near-field optical microscopy (s-

* Special Topic: Two-dimensional Layered Materials and Device Physics (Ed. Lei Wang). This article can also be found at http://journal.hep.com.cn/fop/EN/10.1007/s11467-021-1140-3.

SNOM). The IR regime is of great interest for graphene, because the energy scales of many physical phenomena and electronic excitations in graphene and related systems lie in this energy range [3], including interband transitions, band gap, many body interactions and collective modes. s-SNOM can provide information about a broad range of electronic phenomena in quantum materials with nanometer spatial resolution [6, 26, 27]. Such high resolution is particularly important for probing the local intrinsic properties of graphene on Cu because measurements on single grain and multiple grains of graphene in this system can show very different results [23, 28, 29]. Moreover, direct imaging of plasmons in graphene requires scanning probes with nanometer resolution. Recently, s-SNOM has been utilized to image and explore plasmons in graphene and related structures [30–42]. However, systematic near-field IR studies of graphene/metal systems have not been reported. One potential challenge is that the strong near-field IR signal of the highly conductive metal substrate [26, 27] may obscure that of graphene, making it difficult to explore graphene using s-SNOM.

In our work, h-BN/Cu samples were firstly measured to study the near-field response of the Cu substrate, which shows edge-fringes formed across the surface steps on Cu [43]. From detailed analysis on the spatial profile of near-field images of graphene/Cu, the near-field response of graphene can be distinguished from that of Cu. Our study reveals three different types of near-field responses in graphene on Cu, which may arise from the modification of optical conductivity of graphene due to doping or strain induced by the substrate.

In our study, near-field imaging is accomplished using an s-SNOM, in which a mid-infrared laser (wavelength of 11 um) focused on the apex of a metallic AFM tip excites a highly localized electromagnetic field in the gap between the tip and the sample due to the antenna effect [26, 27, 44, 45]. This localized field decays exponentially normal to the sample surface within tens to hundreds of nanometers [27]. The AFM tip is operated in tapping mode and the tip-scattered light is measured at far field by a detector, as shown in Fig. 1. To identify the near-field signal which encodes the electronic and optical properties of sample surface, a pseudo-heterodyne interferometry and demodulation of detected signal at 3rd harmonic of tip resonance frequency have been implemented. The magnitude of near-field amplitude signal is proportional to the vertically effective polarizability of tip which is determined by the tip-sample coupling strength and optical constants of the sample [26, 27, 44, 45].

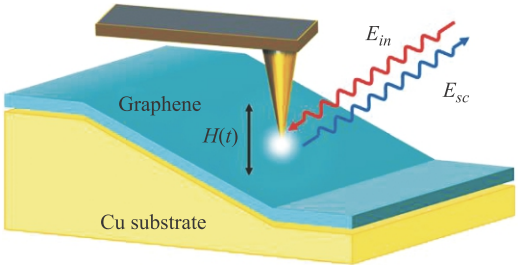

Fig. 1 Schematic of s-SNOM. A mid-infrared laser is focused on the apex of a metallic AFM tip, which oscillates vertically with amplitude A and frequency Ω. The tip-sample separation is $H(t) = H_0 + A[1 + \cos(\Omega t)]$, where H_0 is the minimum tip-sample separation. E_{in}: Incident light; E_{sc}: Scattered light.

The high-quality graphene/Cu and h-BN/Cu samples were obtained by means of CVD growth technique. For graphene/Cu samples [20–22], the industrial copper foil (25 μm thick, 99.8% purity) was placed horizontally on CVD tube furnace, and heated up to 1020 °C under reducing gases Ar and H_2 of 500 sccm and 10 sccm, respectively. The furnace was kept at same temperature for 30 minutes, then the monocrystal Cu substrate was obtained. The CH_4 (1 [ ]sccm) gas was introduced to the furnace to grown graphene samples. After growth process, the samples were cooled naturally to room temperature under the reducing gases condition mentioned above. Raman spectroscopy showed that the samples are single layer graphene. The h-BN/Cu samples were obtained by the method in Ref. [46].

3 Results and discussion

First, h-BN/Cu samples were measured to study the near-field response of the Cu substrate. h-BN/Cu samples were chosen because h-BN can protect the Cu substrate from oxidation in ambient condition. Moreover, h-BN does not modify the near-field response of the Cu substrate because our laser frequency is far from the phonons of h-BN47. Figure 2(a) shows the AFM topography and near-field amplitude image of a region in the vicinity of a step on h-BN/Cu. The step originates from the surface topography of Cu substrate. While the near-field amplitude image of h-BN/Cu shows constant at the low and high plateaus of the step, a peak and a dip were observed in the near-field amplitude near the edge of the step, as indicated by the 1st and 2nd vertical dash lines in Fig. 2(a) respectively. The full width of the dip feature between the 1st and 3rd vertical dash lines is similar to the width of the edge.

Remarkably, three significantly different types of responses were observed in the near-field amplitude image of graphene/Cu near steps on the substrate, as shown in Figs. 2(b)–(d). In some samples, a pronounced peak and dip feature [Fig. 2(b)] were observed (refer to as the "peak-dip" case) corresponding to the lower and upper of ends of the edge of the step, respectively. In the second type of response (the "peak" case) shown in Fig. 2(c), a single peak was observed corresponding to the lower end of the edge and the signals at the low and high plateaus of the step remain constant. Lastly, a third type of response (the

"dip" case) was observed featuring a single dip inside the edge of the step as shown in Fig. 2(d).

For non-resonant materials such as h-BN at laser wavelength far from its phonon frequency, prior studies [43] have demonstrated that the emergence of a "peak-dip" feature in near-field amplitude near a surface step can be explained based on the geometries of the step. The process of a tip scanning across a h-BN/Cu step can be divided into four stages [43] as labeled in Fig. 3(a): (i) When the tip is located in the low plateau of the step, a hot-spot48 is excited by the external field of the excitation laser and formed under the tip apex [43, 49], which is a local region where the intensity of electromagnetic field is highly localized and very strong. The field of the hot-spot is scattered by the tip into the far field, producing signal seen in s-SNOM. The near-field amplitude in this region is constant due to the homogeneity of the sample. (ii) When the tip approaches and contacts the edge of step, two hot-spots are formed, one under the tip apex and another at the gap between the edge of step and the side of tip, as indicated by black arrows in schematic in Fig. 3(b). Because the intense optical field of a hot-spot gives rise to strong near field signal, the formation of two hot-spots strongly enhances the near-field amplitude in stage (ii) compared to region ①. Thus, a peak appears in the near-field amplitude as shown in Fig. 2(a) label ②. (iii) When the apex of the tip is located above the edge of the step, the hot-spot under the tip apex disappears due to the lack of contact with the sample, and only one hot-spot remains between the side of the tip and the edge of the step. Because the overall effective polarizability of the tip is vertical, the local field enhancement from the hot-spot at the side of the tip is weaker than that from the hot-spot under the tip apex. The weaker field enhancement of the former leads to a decrease in the near-field amplitude in stage (iii) compared to that in stage (i), so a dip appears in the near-field amplitude as shown in Fig. 2(a) label ③. (iv) When the tip is scanned away from the edge and enters the high plateau, one hot-spot is formed under the tip apex again, so the near-field amplitude is similar to that of stage (i). As shown in Fig. 3, the near-field response of h-BN/Cu can be explained by this picture.

For graphene/Cu samples, the near-field amplitude with "peak-dip" feature is notably different from the response of h-BN/Cu. While the full width of the dip feature in h-BN/Cu is similar to the width of the edge [Fig. 2(a)], the dip feature in graphene/Cu is much wider spatially compared to the width of the edge [Fig. 2(b)]. In the latter case, the dip feature extends far into the high plateau region spatially. For the "peak" case in graphene/Cu, only a single peak is observed as shown in Fig. 2(c), whereas only a single dip is observed inside the edge of the step for the "dip" case [Fig. 2(c)]. All these three types of near-field responses of graphene/Cu are completely different from that of the Cu substrate.

Next, we verify whether the three types of near-field responses in graphene/Cu samples are related to the geometries of steps on Cu. An examination on the width

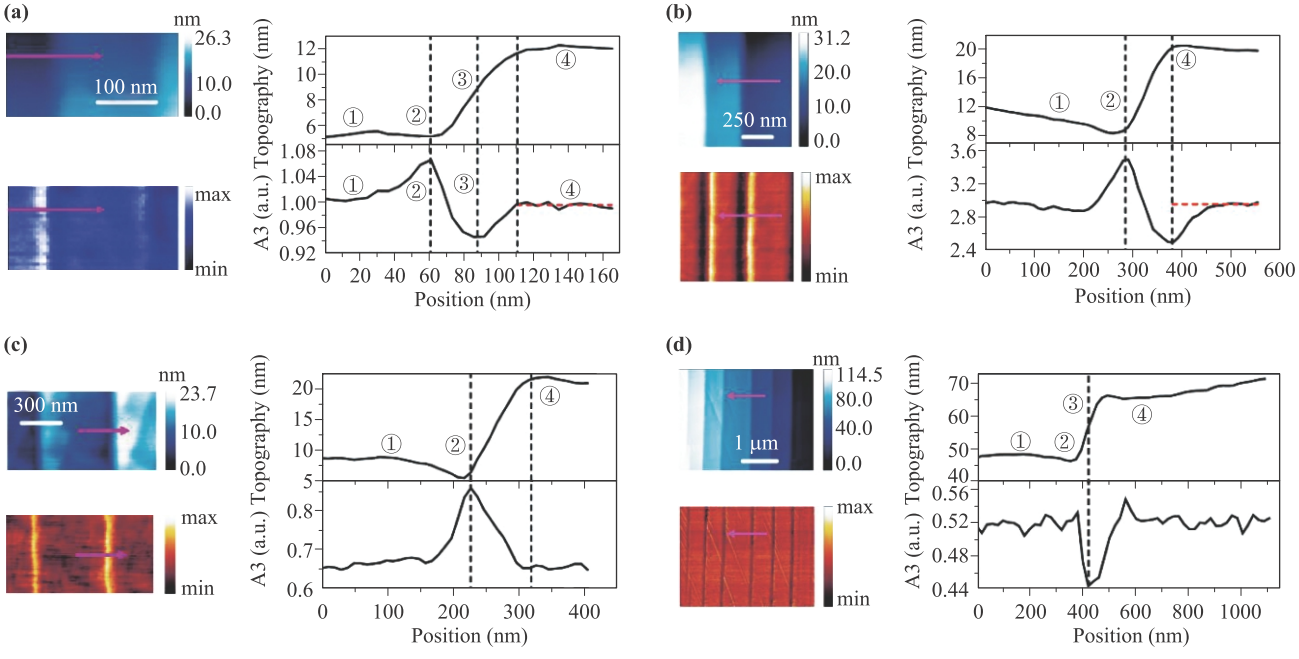

Fig. 2 Topography and near-field amplitude images of h-BN/Cu **(a)** and graphene/Cu **(b–d)**. Line-profiles in each part are topography and near-field amplitude corresponding to the magenta arrows. The red dash lines represent the constant near-field amplitude at the topographic plateaus. The labeled numbers indicate the representative stages of the tip scanning across a surface step.

and height of surface steps measured in this study (Fig. 4) shows that the shape (height-width ratio) of various steps for the three types of responses are very close to one another, suggesting that our observations are approximatively independent on the shape of the step. Furthermore, if the near-field response is related to the geometries of steps, two steps with similar width and height should show similar near-field amplitude features. In stark contrast, we find that two different steps with similar width and height on graphene/Cu can show very different near-field amplitude features, as indicated by two magenta circles in Fig. 4. In particular, two different steps with width and height of about 100 nm and 10 nm show "peak-dip" and "peak" features, respectively; another two steps with width and height of about 120 nm and 17 nm show "peak" and "dip" features, respectively. Therefore, our study has unambiguously demonstrated that the three types of near-field responses shown in Figs. 2(b–d) arise from the near-field response of graphene instead of from surface steps on Cu.

It has been shown that Cu substrate can introduce doping and strain in graphene [50, 51]. Charge transfer between graphene and Cu substrates can lead to doping in graphene, which depends on the lattice orientation of Cu substrates [50, 51]. On the other hand, the different coefficients of thermal expansion between graphene and Cu substrates [52, 53] can induce strain in graphene during cooling process in CVD growth, so graphene could be subject to different strain at different areas of the step. The applied strain makes the optical conductivity of graphene deviating from a universal and isotropic value [54]. Recent *ab initio* calculation [55] has shown that the optical conductivity of strained graphene in the infrared range is sensitive to the amount of strain. Especially, for the uniaxial strained graphene, the optical conductivity in the parallel (perpendicular) direction to the strain decreases (increases) with increasing the amount of strain and the optical conductivity in two directions change by the same amount [55, 56]. So it is anticipated that strain could modify the local optical conductivities of different areas of graphene.

Substrate induced doping and strain can modify the local optical conductivity of graphene in different areas of the sample [40, 56] and consequently impact the near-field response of graphene, which is approximately proportional to its optical conductivity [37, 38]. When the tip-sample coupling is non-resonant, the SNOM response $s(\omega)$ within the point-dipole approximation can be calculated from the frequency- and momentum-(q) dependent P-polarized reflection coefficient $r_p(q,\omega)$ of the system convoluted with a near-field weight function of the form $q^2\exp(-2qz_{\rm d})$, where $z_{\rm d}$ is the distance between the tip dipole and the surface [37, 38]. The dominant in-plane momenta contributing to near-field coupling are distributed around $q^* = 1/R \sim 3\times10^5$ cm^{-1}, where R is the AFM tip radius. Here $r_p(q,\omega)$ describes electrodynamics of the system in the near field, namely, evanescent fields with large in-plane momenta q. Around the momentum q^* at a fixed frequency, it has been shown that to first order approximation $r_p \approx r_\infty - A\sigma$ [38], where $r_\infty = r_p$ $(q\to\infty)$, A is a constant related to the permittivity parameters of the system and σ is the optical conductivity of graphene. Therefore, the presence of the graphene leads to a change of near field signal proportional to its local conductivity, which has been observed in previous SNOM measurements [38]. In the "peak-dip" case observed in the near field imaging of graphene/Cu, the extension of the dip feature far into the high plateau region might be attributed to decreased optical conductivity of graphene in this region due to substrate induced strain or doping, which leads to decreased near-field amplitude in the high plateau. Similarly, the absence of a peak feature in the "dip" case may arise from decreased optical conductivity of graphene at the low end of the edge in that case caused by the substrate. On the other hand, the absence of dip feature in the "peak" case might originate from enhanced optical conductivity of graphene in the edge of the step in that case due to strain or doping, which increases the near-field amplitude and compensates the dip feature in the edge expected from the substrate alone. Therefore, the diverse near-field responses of graphene/Cu observed in our study can be naturally explained by substrate induced doping and strain, which can vary considerably in

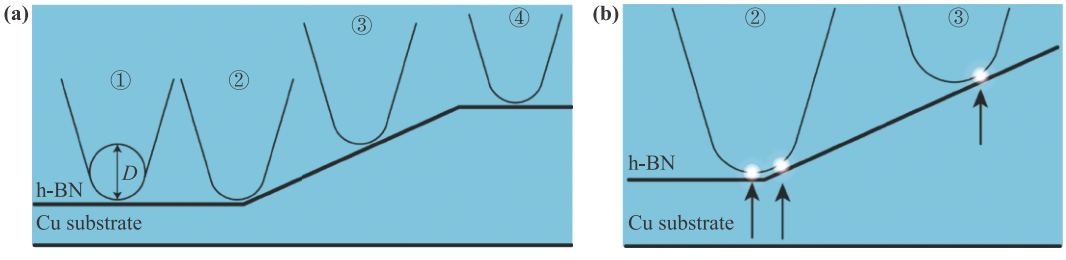

Fig. 3 **(a)** Four stages when a tip is scanned across a surface step. The circle drawn on the tip represents its apex with diameter of D. **(b)** Zoom-in on the gap between the tip and sample surface at positions ② and ③. The white fuzzy regions and black arrows indicate hot-spots.

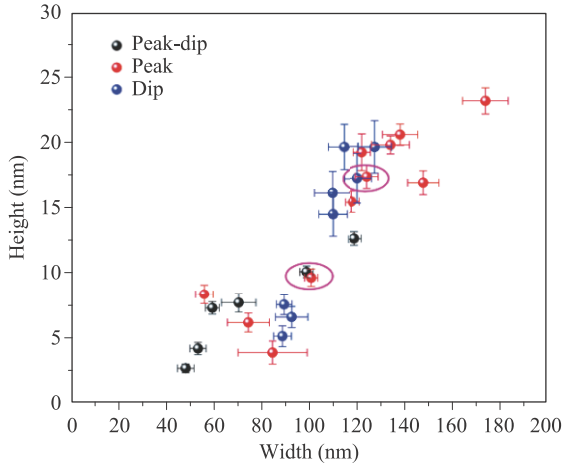

Fig. 4 The width and height of various surface steps on graphene/Cu samples measured in this study. Two different steps with similar width and height can show different types of near field responses, as indicated by the magenta circles.

different samples. Further studies on the detailed distribution of doping and strain near the steps on the substrate are beyond the scope of the present work.

4 Summary

In summary, we have demonstrated a viable approach for identifying the near-field IR response of graphene in graphene/metal systems. Three significantly different types of near-field profiles are observed in graphene on Cu, which may be attributed to the modification of optical conductivity of graphene due to substrate-induced doping or strain. Our study provides a qualitative framework for identifying the near-field IR response of graphene on metal substrate and lays the groundwork for revealing the novel physics therein.

Acknowledgements This work was supported by the National Natural Science Foundation of China (Grant No. 11874271).

References

1. A. H. Castro Neto, F. Guinea, N. M. R. Peres, K. S. Novoselov, and A. K. Geim, The electronic properties of graphene, *Rev. Mod. Phys.* 81(1), 109 (2009)
2. V. N. Kotov, B. Uchoa, V. M. Pereira, F. Guinea, and A. H. Castro Neto, Electron–electron interactions in graphene: Current status and perspectives, *Rev. Mod. Phys.* 84(3), 1067 (2012)
3. D. N. Basov, M. M. Fogler, A. Lanzara, F. Wang, and Y. Zhang, Graphene spectroscopy, *Rev. Mod. Phys.* 86(3), 959 (2014)
4. D. M. Basko and I. L. Aleiner, Interplay of Coulomb and electron–phonon interactions in graphene, *Phys. Rev. B* 77(4), 041409 (2008)
5. M. Lazzeri, C. Attaccalite, L. Wirtz, and F. Mauri, Impact of the electron-electron correlation on phonon dispersion: Failure of LDA and GGA DFT functionals in graphene and graphite, *Phys. Rev. B*78(8), 081406 (2008)
6. D. N. Basov, M. M. Fogler, and F. J. García de Abajo, Polaritons in van der Waals materials, *Science* 354(6309), aag1992 (2016)
7. A. N. Grigorenko, M. Polini, and K. S. Novoselov, Graphene plasmonics, *Nat. Photonics* 6(11), 749 (2012)
8. T. Low and P. Avouris, Graphene plasmonics for terahertz to mid-infrared applications, *ACS Nano* 8(2), 1086 (2014)
9. A. Principi, R. Asgari, and M. Polini, Acoustic plasmons and composite hole-acoustic plasmon satellite bands in graphene on a metal gate, *Solid State Commun.* 151(21), 1627 (2011)
10. T. Stauber and G. Gómez-Santos, Plasmons in layered structures including graphene, *New J. Phys.* 14(10), 105018 (2012)
11. X. F. Gu, I. T. Lin, and J. M. Liu, Extremely confined terahertz surface plasmon-polaritons in graphene-metal structures, *Appl. Phys. Lett.* 103, 071103 (2013)
12. P. Alonso-González, A. Y. Nikitin, Y. Gao, A. Woessner, M. B. Lundeberg, A. Principi, N. Forcellini, W. Yan, S. Vélez, A. J. Huber, K. Watanabe, T. Taniguchi, F. Casanova, L. E. Hueso, M. Polini, J. Hone, F. H. L. Koppens, and R. Hillenbrand, Acoustic terahertz graphene plasmons revealed by photocurrent nanoscopy, *Nat. Nanotechnol.* 12(1), 31 (2017)
13. M. B. Lundeberg, Y. D. Gao, R. Asgari, C. Tan, B. Van Duppen, M. Autore, P. Alonso-Gonzalez, A. Woessner, K. Watanabe, T. Taniguchi, R. Hillenbrand, J. Hone, M. Polini, and F. H. L. Koppens, Tuning quantum nonlocal effects in graphene plasmonics, *Science* 357(6347), 187 (2017)
14. A. Principi, E. van Loon, M. Polini, and M. I. Katsnelson, Confining graphene plasmons to the ultimate limit, *Phys. Rev. B* 98(3), 035427 (2018)
15. A. Rodríguez Echarri, J. D. Cox, and F. J. García de Abajo, Quantum effects in the acoustic plasmons of atomically thin heterostructures, *Optica* 6(5), 630 (2019)
16. S. H. Choi, Y. L. Kim, and K. M. Byun, Graphene-on-silver substrates for sensitive surface plasmon resonance imaging biosensors, *Opt. Express* 19(2), 458 (2011)
17. O. Salihoglu, S. Balci, and C. Kocabas, Plasmon-polaritons on graphene-metal surface and their use in biosensors, *Appl. Phys. Lett.* 100(21), 213110 (2012)
18. D. Rodrigo, O. Limaj, D. Janner, D. Etezadi, F. J. García de Abajo, V. Pruneri, and H. Altug, Mid-infrared plasmonic biosensing with graphene, *Science* 349(6244), 165 (2015)
19. F. H. L. Koppens, T. Mueller, P. Avouris, A. C. Ferrari, M. S. Vitiello, and M. Polini, Photodetectors based on graphene, other two-dimensional materials and hybrid systems, *Nat. Nanotechnol.* 9(10), 780 (2014)

20. X. Xu, Z. Zhang, L. Qiu, J. Zhuang, L. Zhang, H. Wang, C. Liao, H. Song, R. Qiao, P. Gao, Z. Hu, L. Liao, Z. Liao, D. Yu, E. Wang, F. Ding, H. Peng, and K. Liu, Ultrafast growth of single-crystal graphene assisted by a continuous oxygen supply, *Nat. Nanotechnol.* 11(11), 930 (2016)
21. X. Xu, Z. Zhang, J. Dong, D. Yi, J. Niu, M. Wu, L. Lin, R. Yin, M. Li, J. Zhou, S. Wang, J. Sun, X. Duan, P. Gao, Y. Jiang, X. Wu, H. Peng, R. S. Ruoff, Z. Liu, D. Yu, E. Wang, F. Ding, and K. Liu, Ultrafast epitaxial growth of metre-sized single-crystal graphene on industrial Cu foil, *Sci. Bull. (Beijing)* 62(15), 1074 (2017)
22. C. Liu, X. Xu, L. Qiu, M. Wu, R. Qiao, L. Wang, J. Wang, J. Niu, J. Liang, X. Zhou, Z. Zhang, M. Peng, P. Gao, W. Wang, X. Bai, D. Ma, Y. Jiang, X. Wu, D. Yu, E. Wang, J. Xiong, F. Ding, and K. Liu, Kinetic modulation of graphene growth by fluorine through spatially confined decomposition of metal fluorides, *Nat. Chem.* 11(8), 730 (2019)
23. J. Avila, I. Razado, S. Lorcy, R. Fleurier, E. Pichonat, D. Vignaud, X. Wallart, and M. C. Asensio, Exploring electronic structure of one-atom thick polycrystalline graphene films: A nano angle resolved photoemission study, *Sci. Rep.* 3(1), 2439 (2013)
24. P. A. Khomyakov, G. Giovannetti, P. C. Rusu, G. Brocks, J. van den Brink, and P. J. Kelly, First-principles study of the interaction and charge transfer between graphene and metals, *Phys. Rev. B* 79(19), 195425 (2009)
25. A. Varykhalov, M. R. Scholz, T. K. Kim, and O. Rader, Effect of noble-metal contacts on doping and band gap of graphene, *Phys. Rev. B* 82(12), 121101 (2010)
26. J. M. Atkin, S. Berweger, A. C. Jones, and M. B. Raschke, Nano-optical imaging and spectroscopy of order, phases, and domains in complex solids, *Adv. Phys.* 61(6), 745 (2012)
27. X. Chen, D. Hu, R. Mescall, G. You, D. N. Basov, Q. Dai, and M. Liu, Modern scattering-type scanning near-field optical microscopy for advanced material research, *Adv. Mater.* 31(24), 1804774 (2019)
28. A. L. Walter, S. Nie, A. Bostwick, K. S. Kim, L. Moreschini, Y. J. Chang, D. Innocenti, K. Horn, K. F. McCarty, and E. Rotenberg, Electronic structure of graphene on single-crystal copper substrates, *Phys. Rev. B* 84(19), 195443 (2011)
29. D. A. Siegel, C. Hwang, A. V. Fedorov, and A. Lanzara, Electron–phonon coupling and intrinsic bandgap in highly-screened graphene, *New J. Phys.* 14(9), 095006 (2012)
30. Z. Fei, A. S. Rodin, G. O. Andreev, W. Bao, A. S. McLeod, M. Wagner, L. M. Zhang, Z. Zhao, M. Thiemens, G. Dominguez, M. M. Fogler, A. H. C. Neto, C. N. Lau, F. Keilmann, and D. N. Basov, Gate-tuning of graphene plasmons revealed by infrared nano-imaging, *Nature* 487(7405), 82 (2012)
31. J. Chen, M. Badioli, P. Alonso-González, S. Thongrattanasiri, F. Huth, J. Osmond, M. Spasenović, A. Centeno, A. Pesquera, P. Godignon, A. Zurutuza Elorza, N. Camara, F. J. G. de Abajo, R. Hillenbrand, and F. H. L. Koppens, Optical nano-imaging of gate-tunable graphene plasmons, *Nature* 487(7405), 77 (2012)
32. J. A. Gerber, S. Berweger, B. T. O′ Callahan, and M. B. Raschke, Phase-resolved surface plasmon interferometry of graphene, *Phys. Rev. Lett.* 113(5), 055502 (2014)
33. S. S. Sunku, G. X. Ni, B. Y. Jiang, H. Yoo, A. Sternbach, A. S. McLeod, T. Stauber, L. Xiong, T. Taniguchi, K. Watanabe, P. Kim, M. M. Fogler, and D. N. Basov, Photonic crystals for nano-light in moiré graphene superlattices, *Science* 362(6419), 1153 (2018)
34. A. Woessner, Y. Gao, I. Torre, M. B. Lundeberg, C. Tan, K. Watanabe, T. Taniguchi, R. Hillenbrand, J. Hone, M. Polini, and F. H. L. Koppens, Electrical 2 phase control of infrared light in a 350-nm footprint using graphene plasmons, *Nat. Photonics* 11(7), 421 (2017)
35. Z. Shi, X. Hong, H. A. Bechtel, B. Zeng, M. C. Martin, K. Watanabe, T. Taniguchi, Y. R. Shen, and F. Wang, Observation of a Luttinger-liquid plasmon in metallic single-walled carbon nanotubes, *Nat. Photonics* 9(8), 515 (2015)
36. G. X. Ni, A. S. McLeod, Z. Sun, L. Wang, L. Xiong, K. W. Post, S. S. Sunku, B. Y. Jiang, J. Hone, C. R. Dean, M. M. Fogler, and D. N. Basov, Fundamental limits to graphene plasmonics, *Nature* 557(7706), 530 (2018)
37. A. Woessner, M. B. Lundeberg, Y. Gao, A. Principi, P. Alonso-González, M. Carrega, K. Watanabe, T. Taniguchi, G. Vignale, M. Polini, J. Hone, R. Hillenbrand, and F. H. L. Koppens, Highly confined low-loss plasmons in graphene–boron nitride heterostructures, *Nat. Mater.* 14(4), 421 (2015)
38. Z. Fei, G. O. Andreev, W. Bao, L. M. Zhang, A. S. McLeod, C. Wang, M. K. Stewart, Z. Zhao, G. Dominguez, M. Thiemens, M. M. Fogler, M. J. Tauber, A. H. Castro-Neto, C. N. Lau, F. Keilmann, and D. N. Basov, Infrared nanoscopy of Dirac plasmons at the graphene–SiO_2 interface, *Nano Lett.* 11(11), 4701 (2011)
39. S. Dai, Q. Ma, M. K. Liu, T. Andersen, Z. Fei, M. D. Goldflam, M. Wagner, K. Watanabe, T. Taniguchi, M. Thiemens, F. Keilmann, G. C. A. M. Janssen, S. E. Zhu, P. Jarillo-Herrero, M. M. Fogler, and D. N. Basov, Graphene on hexagonal boron nitride as a tunable hyperbolic metamaterial, *Nat. Nanotechnol.* 10(8), 682 (2015)
40. G. X. Ni, H. Wang, J. S. Wu, Z. Fei, M. D. Goldflam, F. Keilmann, B. Özyilmaz, A. H. Castro Neto, X. M. Xie, M. M. Fogler, and D. N. Basov, Plasmons in graphene moiré superlattices, *Nat. Mater.* 14(12), 1217 (2015)
41. B. Y. Jiang, G. X. Ni, Z. Addison, J. K. Shi, X. Liu, S. Y. F. Zhao, P. Kim, E. J. Mele, D. N. Basov, and M. M. Fogler, Plasmon reflections by topological electronic boundaries in bilayer graphene, *Nano Lett.* 17(11), 7080 (2017)
42. L. Jiang, Z. Shi, B. Zeng, S. Wang, J. H. Kang, T. Joshi, C. Jin, L. Ju, J. Kim, T. Lyu, Y. R. Shen, M. Crommie, H. J. Gao, and F. Wang, Soliton-dependent plasmon reflection at bilayer graphene domain walls, *Nat. Mater.* 15(8), 840 (2016)
43. V. E. Babicheva, S. Gamage, M. I. Stockman, and Y. Abate, Near-field edge fringes at sharp material boundaries, *Opt. Express* 25(20), 23935 (2017)

44. B. Y. Jiang, L. M. Zhang, A. H. C. Neto, D. N. Basov, and M. M. Fogler, Generalized spectral method for near-field optical microscopy, *J. Appl. Phys.* 119(5), 054305 (2016)
45. A. S. McLeod, P. Kelly, M. D. Goldflam, Z. Gainsforth, A. J. Westphal, G. Dominguez, M. H. Thiemens, M. M. Fogler, and D. N. Basov, Model for quantitative tip-enhanced spectroscopy and the extraction of nanoscale-resolved optical constants, *Phys. Rev. B* 90(8), 085136 (2014)
46. L. Wang, X. Z. Xu, L. N. Zhang, R. X. Qiao, M. H. Wu, Z. C. Wang, S. Zhang, J. Liang, Z. H. Zhang, Z. B. Zhang, W. Chen, X. D. Xie, J. Y. Zong, Y. W. Shan, Y. Guo, M. Willinger, H. Wu, Q. Y. Li, W. L. Wang, P. Gao, S. W. Wu, Y. Zhang, Y. Jiang, D. P. Yu, E. G. Wang, X. D. Bai, Z. J. Wang, F. Ding, and K. H. Liu, Epitaxial growth of a 100-square-centimetre single-crystal hexagonal boron nitride monolayer on copper, *Nature* 570(7759), 91 (2019)
47. X. Yang, F. Zhai, H. Hu, D. Hu, R. Liu, S. Zhang, M. Sun, Z. Sun, J. Chen, and Q. Dai, Far-field spectroscopy and near-field optical imaging of coupled plasmon-phonon polaritons in 2D van der Waals heterostructures, *Adv. Mater.* 28(15), 2931 (2016)
48. L. Novotny and B. Hecht, Principles of Nano-Optics, Cambridge University Press, Cambridge, 2006
49. Y. Abate, S. Gamage, Z. Li, V. Babicheva, M. H. Javani, H. Wang, S. B. Cronin, and M. I. Stockman, Nanoscopy reveals surface-metallic black phosphorus, *Light Sci. Appl.* 5(10), e16162 (2016)
50. O. Frank, J. Vejpravova, V. Holy, L. Kavan, and M. Kalbac, Interaction between graphene and copper substrate: The role of lattice orientation, *Carbon* 68, 440 (2014)
51. S. D. Costa, J. Ek Weis, O. Frank, and M. Kalbac, Temperature and face dependent copper–graphene interactions, *Carbon* 93, 793 (2015)
52. W. Bao, F. Miao, Z. Chen, H. Zhang, W. Jang, C. Dames, and C. N. Lau, Controlled ripple texturing of suspended graphene and ultrathin graphite membranes, *Nat. Nanotechnol.* 4(9), 562 (2009)
53. D. Yoon, Y. W. Son, and H. Cheong, Negative thermal expansion coefficient of graphene measured by Raman spectroscopy, *Nano Lett.* 11(8), 3227 (2011)
54. M. Oliva-Leyva and G. G. Naumis, Anisotropic AC conductivity of strained graphene, *J. Phys.: Condens. Matter* 26(12), 125302 (2014)
55. V. M. Pereira, R. M. Ribeiro, N. M. R. Peres, and A. H. Castro Neto, Optical properties of strained graphene, *EPL (Europhys. Lett.)* 92(6), 67001 (2010)
56. G. G. Naumis, S. Barraza-Lopez, M. Oliva-Leyva, and H. Terrones, Electronic and optical properties of strained graphene and other strained 2D materials: A review, *Rep. Prog. Phys.* 80(9), 096501 (2017)